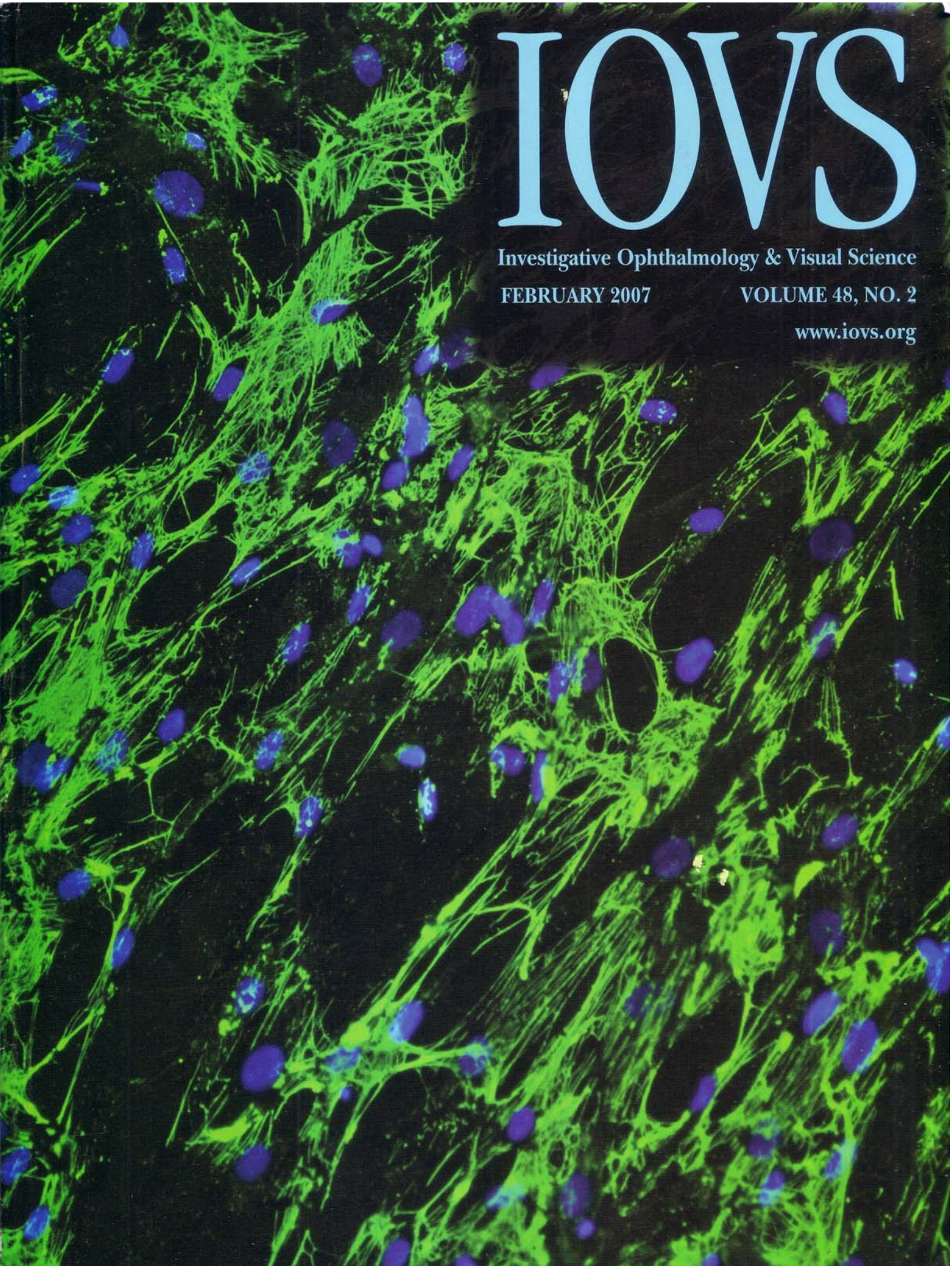

IOVS

Investigative Ophthalmology & Visual Science

FEBRUARY 2007 VOLUME 48, NO. 2

www.iovs.org

Stimulation via a Subretinally Placed Prosthetic Elicits Central Activity and Induces a Trophic Effect on Visual Responses

Paul J. DeMarco, Jr,[1,2] *Gary L. Yarbrough,*[2] *Christopher W. Yee,*[2] *George Y. McLean,*[3] *Botir T. Sagdullaev,*[2,4] *Sherry L. Ball,*[5] *and Maureen A. McCall*[2,6]

Purpose. Subretinal prosthetics are designed to electrically stimulate second-order cells, replacing dysfunctional photoreceptors in diseases such as retinitis pigmentosa (RP). For functional vision to occur, this signal must also reach central visual structures. In the current study, a subretinally implanted prosthetic was evaluated in the Royal College of Surgeons (RCS) rat model of RP, to determine its capacity to activate the retinotectal pathway.

Methods. Prosthetic implants were placed in RCS and wild-type (WT) rats at 4 weeks of age and evaluated 3 months later. Control rats underwent sham surgery, implantation with inactive prosthetics, or no treatment. Implant- and visible-evoked responses were isolated and evaluated in the superior colliculus (SC).

Results. In WT and RCS rats with active prosthetics, implant-driven responses were found in 100% of WT and 64% of RCS rats and were confined to a small SC region that corresponded to the retinal sector containing the implant and differed from visible-evoked responses. In addition, visible-evoked responses were more robust at sites that received implant input compared to sites that did not. These effects were not seen in WT rats or RCS control animals; although a general trophic effect on the number of responsive sites was observed in all RCS rats with surgery compared to untreated RCS rats.

Conclusions. Direct activation of the retina by a subretinal implant induces activity in the SC of RCS rats, suggesting that these implants have some capacity to replace dysfunctional photoreceptors. The data also provide evidence for implant-induced neurotrophic effects as a consequence of both its presence and its activity in the retina. (*Invest Ophthalmol Vis Sci.* 2007;48:916–926) DOI:10.1167/iovs.06-0811

From the [1]Louisville VA Medical Center, the Departments of [2]Psychological and Brain Sciences and [6]Ophthalmology and Visual Sciences, University of Louisville, Louisville, Kentucky; [3]Optobionics Corp., Palo Alto, California; and the [5]Cleveland VA Medical Center, Cleveland, Ohio.

[4]Present affiliation: Department of Ophthalmology Visual Science, Washington University, St. Louis MO.

Supported by a contract with Optobionics, Corp. (MAMcC, PJDeM), the Department of Veterans Affairs (PJDeM, SLB) and by NIH R01 EY014701 (MAMcC).

Submitted for publication July 14, 2006; revised August 11 and 28, 2006; accepted December 15, 2006.

Disclosure: **P.J. DeMarco, Jr**, None; **G. L. Yarbrough**, None; **C.W. Yee**, None; **G.Y. McLean**, Optobionics Corp. (P, E); **B.T. Sagdullaev**, None; **S.L. Ball**, None; **M.A. McCall**, None

The publication costs of this article were defrayed in part by page charge payment. This article must therefore be marked "*advertisement*" in accordance with 18 U.S.C. §1734 solely to indicate this fact.

Corresponding author: Maureen A. McCall, Department of Psychological and Brain Sciences, 317 Life Sciences Building, University of Louisville, Louisville, KY 40292; mo.mccall@louisville.edu.

In the human population, diseases such as retinitis pigmentosa (RP) and age-related macular degeneration (AMD) result from a loss of photoreceptor cells causing visual impairment and blindness. Animal models are available for many of these diseases and have been used to develop therapeutic strategies.[1,2] One popular small mammal model of RP is the rat, with three frequently used strains: Royal College of Surgeons (RCS) and the S334ter and P23H transgenic lines. For all, both the etiology and the time course of photoreceptor degeneration differ. The RCS phenotype results from defective gene expression in the *MERTK* gene in the pigment epithelium,[3] whereas the transgenic models cause expression of two mutant forms of the rhodopsin pigment.[4]

Treatment strategies to ameliorate photoreceptor degeneration are diverse and include exploration of survival or growth factors,[5–7] gene therapies[8–11]; somatic cell, tissue,[12,13] or stem cell transplantation therapies[14,15]; and modification of retinal metabolism.[16] Each approach shows promise but has limitations. Gene therapy with recombinant adenoviral or adenoviral-associated viral vectors has arrested degeneration and loss of visual function in animal models of RP.[17–27] However, the genetic heterogeneity that underlies the diverse mechanisms that cause photoreceptor degeneration limits the feasibility of this strategy to the most common genetic forms of the disease. Although there are many other approaches that have successfully slowed or arrested photoreceptor cell death,[5,26,28–45] functional rescue has had more mixed results.[32,46–48] In addition, for some transplantation approaches there are ethical issues involving the procurement of human tissue.[15,49,50]

A different strategy that has the potential for more universal application and circumvents ethical issues is the replacement of dysfunctional or degenerated photoreceptors by sub- and/or epiretinal prosthetic devices. Electrical stimulation has been shown to produce phosphenes when applied externally to the eye in normal human subjects.[51–53] More recently, intraocular electrical stimulation of the retinal nerve fiber layer has also been shown to evoke phosphenes and/or perception of patterns in RP patients.[54–58] In vitro and in vivo animal studies also show that electrical activity in the retina can be induced by electrical stimulation of the outer retina,[59–62] the eye globe,[63] or ganglion cell/nerve fiber layer.[64–67] As a consequence, various retinal prosthetic designs are under development,[68,69] including epiretinal,[54,58,70–73] suprachoroidal,[74] and subretinal devices.[59,74–77] All are designed to produce an electric current in response to light stimulation, either directly or via an external power supply or to change the membrane potential of neurons to replace or augment their synaptic activation. Thus, epiretinal designs are able to provide stimulation of the ganglion cells and/or their nerve fibers that appear to remain viable until late in the degenerative process.[78] In contrast, subretinal designs use the remaining retinal circuitry to shape the transmitted signal, making it more similar to the native signal.

One subretinal implant, the Artificial Silicon Retina (ASR; Optobionics, Inc., Palo Alto, CA),[75] is a self-powered device

that consists of a microphotodiode array. As used in rodents, the ASR is 1 mm in diameter and 25 μm thick and contains approximately 1200 electrodes. Its long-term biocompatibility has been demonstrated in humans, cats, and rodents (Faulkner A et al. *IOVS* 2005;46:ARVO E-Abstract 1518).[79–81] The implant is designed so that each microphotodiode can transduce light into an electric current independently at each electrode, although other factors, such as distance to the target tissue, also are relevant. Introduction of this design created a controversy in the literature regarding its ability to generate sufficient current to produce a biologically relevant signal.[82–84] However, there has been no empirical evaluation of the performance of such a device design. To this end, we implanted the ASR device in RCS rats and evaluated its ability to produce a signal in the superior colliculus (SC) when the device was stimulated in situ. The SC was chosen because it receives a direct synaptic input from the retina that is topographically mapped onto its dorsal surface.

In the present study, the data show that full-field retinal stimulation created a current in a subretinally implanted device and evoked a neural response in the SC. Further, there was both a general effect of surgery on overall visual responsiveness in the SC and a specific effect of the presence of an active implant on the characteristics of visual responses. These data represent an important characterization of the direct output of a subretinally placed implant, as well as the separation of its direct effects from more indirect, trophic effects on the retinal circuit. Further, they are a crucial first step in the refinement of subretinally placed prosthetic devices to replace dysfunctional and/or degenerated photoreceptors.

Methods

Experimental Animals

All experiments were approved by either the University of Louisville or the Cleveland VA Medical Center (VAMC) Institutional Animal Care and Safety Committee and were in compliance with the ARVO Statement for the Use of Animals in Ophthalmic and Vision Research. Pigmented RCS and Long Evans rats were used as the experimental model of RP and wild-type (WT) controls, respectively (http://ucsfeye.net/mlavailRDratmodels.shtml/ and Harlan Sprague-Dawley, Inc., http://www.harlan.com). Table 1 delineates the experimental and control groups that were used in these experiments. In the two experimental conditions, RCS (n = 14) and WT (n = 5) rats' eyes were implanted with active devices. In the control conditions, RCS rats received inactive devices, underwent implant surgery without implant placement, or received no treatment. All implant surgeries were performed at the Cleveland VAMC, and the rats were shipped to the University of Louisville for functional evaluation.

Subretinal Implant Placement

Rats were implanted with ASR devices between 28 to 35 days of age, as described previously.[85,86] Anesthesia was induced with an IP injection of ketamine-xylazine (37.5; 5 mg/kg). The pupil of the eye was dilated with 1% tropicamide and 2.5% phenylephrine HCl eye drops, and the ocular surface was anesthetized with 1% proparacaine HCl. A suture, placed in the superior limbus of the eye was used to rotate and expose the back of the eye. A 1.5-mm incision was made through all layers in the superior/nasal orbit and once the retina detached at the incision site, the ASR was slid gently into the subretinal space. After placement was complete, ophthalmic antibiotic was applied, the suture was removed, and the eye was rotated back to its original position. Table 1 describes the age of postsurgical assessment for each group.

Light Stimulation

Light stimuli were presented in the presence of room lighting, which produced a background luminance of 2.3 cd/m^2 and were delivered via a custom-designed device containing interleaved arrays of either blue (λ_{max} = 469 nm) or infrared (IR: λ_{max} 851 nm) light-emitting diodes (LEDs). The LED array was covered with diffusing glass, and light exited through an aperture 2.5 cm in diameter, producing a spatially uniform field that subtended approximately 80° of visual angle, with the device positioned 0.5 cm in front of the rat's eye. Stimulus duration (200 ms) and intensity were controlled by a voltage-to-current driver interfaced with a data acquisition system (National Instruments, Austin, TX).

Figure 1 is a plot of the spectral responsivity of the ASR and the three rat photopigments. The graph illustrates that the implant was only slightly less sensitive to blue (visible) than to IR stimuli, and rat photoreceptors were very insensitive in the IR stimulus range. The relative spectral profiles of the visible and IR LED stimuli used in this study also are shown in Figure 1. Stimulus irradiances of the IR and visible stimuli are 87 mW · cm^{-2} and 2.7 mW · cm^{-2}, respectively. Our calculations (Table 2) suggest that our IR stimulus produces a photocurrent in the implant that is approximately 50 times greater than the current produced using our visible stimulus. Because the visible stimulus also excites photoreceptors, we report its luminance, taking into account its duration (200 ms), which is 92 cd · s/m^2.

Electrophysiological Assessment of Stimulation-Induced Responses in the Superior Colliculus

The preparation for electrophysiological assessments has been described previously,[87,88] as has the rationale for evaluating responses in the SC. Briefly, the SC is a central visual structure that receives a direct retinal input across its dorsal surface that contains an orderly retinotopic map.[89,90] Thus, one can correlate areas of SC activity with the location of the implant in the retina (in these experiments, the superior-nasal quadrant).

Anesthesia was induced, as described for implant surgery, and the rat was placed in a stereotaxic apparatus. A cone (Stoelting Co., Chicago, IL) was placed and sealed over its nose, and a gas inhalant anesthetic (1.0%–2.0% halothane in 40% O_2/60% N_2O) maintained anesthesia throughout the remainder of the experiment. A craniotomy was performed, and the overlying cortex removed to expose the SC. Extracellular multiunit responses to full-field visual stimulation were recorded systematically across the dorsal surface of the SC, using

Table 1. Overview of Animals Used in the Experiments

Experimental and Control Groups	n	Recording Age (mo)	
		Range	Mean
WT rats, untreated	9	1.1–5.9	2.7
WT rats, active implants	5	3.1–6.6	5.1
RCS rats, active implants with infrared responses	9	4.0–7.4	4.9
RCS rats, active implants without infrared responses	5	3.0–5.1	4.1
RCS rats, untreated	9	3.4–5.9	5.0
RCS rats, sham surgery	7	2.1–4.8	3.8
RCS rats, inactive implants	4	3.0–6.2	4.4

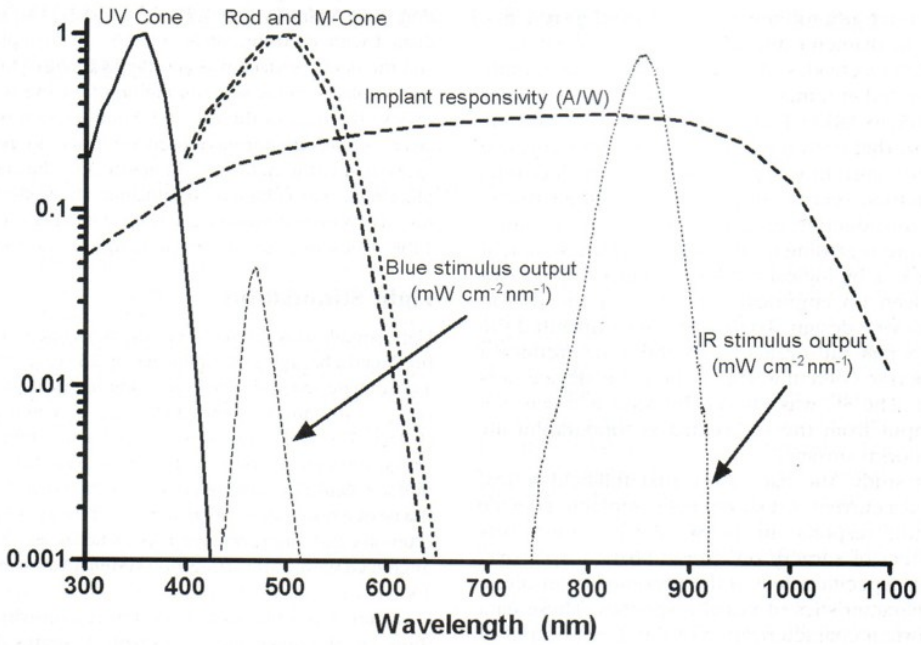

FIGURE 1. Profiles of the spectral sensitivities of rat photoreceptors, the ASR device, and the IR and visible stimuli. The spectral sensitivities of rat rod and UV- and M-cone photoreceptors normalized to their own peak sensitivities are plotted as a function of wavelength. The responsivity of the ASR device at 635 nm was measured directly in an in vitro preparation, and the responsivity at all other wavelengths was estimated by interpolation, using measurements of two test structures fabricated on the same substrate as the ASR device: (1) a large photodiode and (2) a pixel array with the same geometry as ASR devices and a direct electrical connection to the front surface electrodes. The emission spectra of the IR and visible LED stimuli also are shown, and the corresponding output at the face of the stimulator is 87 and 2.7 mW/cm^2, respectively (see also Table 2). The *y*-axis is unlabeled because three different sets of units are represented in the plot: the normalized sensitivities of the photoreceptors, the ASR device responsivity ($A \cdot W^{-1}$) and the emission spectra ($mW \cdot cm^{-2} \cdot nm^{-1}$); however, its numerical values apply to all six curves.

parylene-coated tungsten microelectrodes (World Precision Instruments, Sarasota, FL) with tip impedances of 1.0 to 1.5 MΩ maximum, at 55 sites on the dorsal surface of the SC, sampled with an intersite spacing of approximately 300 μm. Sampling began at the lateral-rostral corner of the SC and progressed systematically to the medial–caudal edge. Sites were skipped only when access was precluded by large blood vessels or the central sinus.

Quantification of Neural Activity in the SC

At each site, both the spontaneous activity and the evoked multiunit activity to IR and visible stimuli were recorded. At each site and for each stimulus and each blank trial (ambient illumination), 16 responses were recorded, and an average response poststimulus time histogram (PSTH) was generated from these raw data (Spike2, ver. 4.02; Cambridge Electronic Design, Cambridge, UK). The average PSTH was used in an analysis program (Labview; National Instruments Inc.) to quantify the response characteristics (the input from retinal ganglion cells to the SC). The analysis program rectified and then smoothed the average waveform, using a triangular moving-average filter (half-width of 2.4 ms; see Fig. 2A).

TABLE 2. Effectiveness of Each Stimulus

	IR	Visible
Subretinal power density (mW/cm^2)	6.5	0.2
ASR device responsivity (A/W)	0.34	0.2
Photocurrent density (mA/cm^2)	2.2	0.04

To quantitatively determine which sites had responses significantly above spontaneous activity and to characterize those responses, we defined two threshold metrics. A high threshold (high) was defined as the mean plus 6 SE above the spontaneous activity. PSTHs with activity that reached or were above this threshold were considered an evoked response. A response duration criterion of >20 ms rejected transient artifacts in the activity. The responses represented by these PSTHs (See Fig. 2B) were characterized using a low threshold (low), defined as the mean plus 2 SE above the spontaneous activity. Response onset latency (onset) was defined as the time after stimulus onset when the activity reached the low threshold criterion. Response duration (*D*) was defined as the point at which the activity no longer exceeded the low threshold, and the total response was computed as the area under the curve above the low-threshold criterion and defined by the onset latency and the response duration. Total response was used to create color-coded surface response maps across the SC for each animal (MatLab, ver. 6.5; MathWorks, Inc., Natick, MA).

Statistical Analyses

All statistical comparisons were made with either a Student's *t*-test or analysis of variance. Significant differences are reported when $P \leq 0.05$. Since IR-evoked responses were recorded only in WT and RCS rats with active implants, these data were compared by Student's *t*-test. When we compared the IR and visible response characteristics recorded in these rats at sites with IR-evoked responses, we used a paired *t*-test and combined the data from WT and RCS rats, since no differences were noted in their IR response characteristics. Sites that had a response to IR stimulation but no response to the visible stimulus were excluded from the analyses so that all comparisons between responses

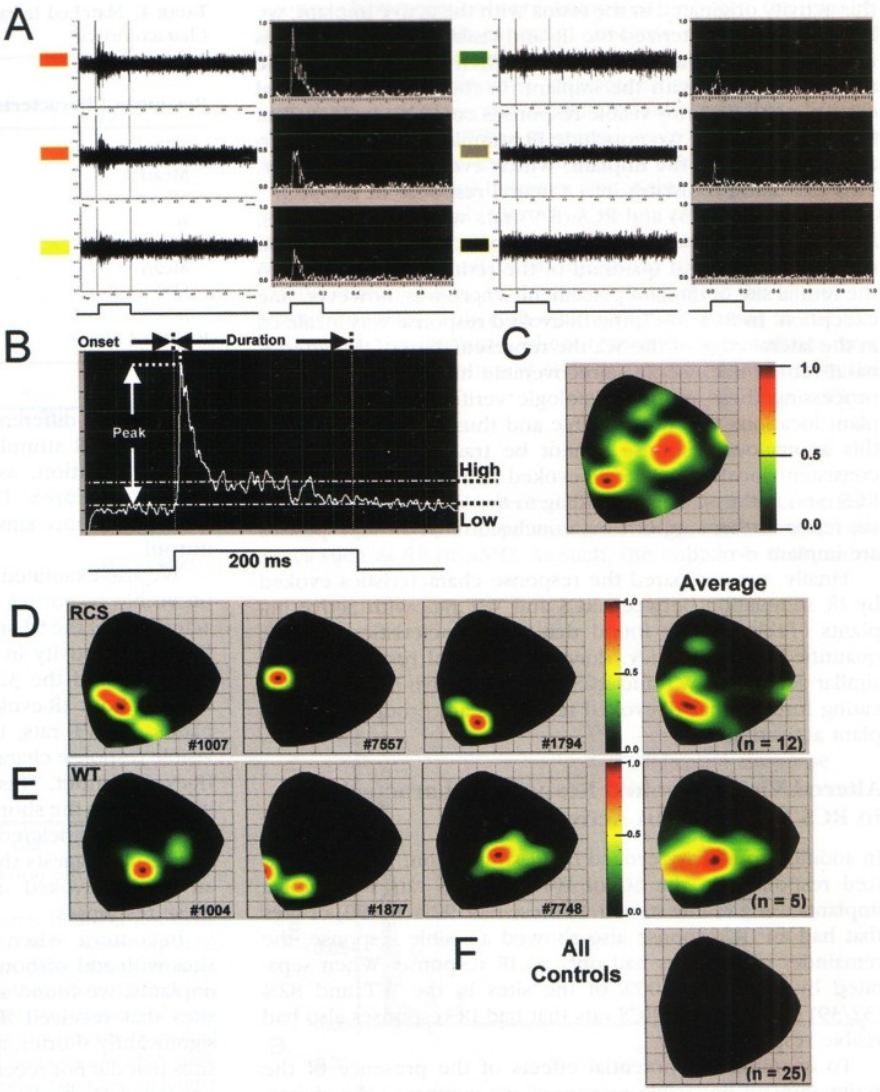

FIGURE 2. Quantification of stimulus-evoked responses, characterization of individual response characteristics, and evidence of direct input from an active subretinal implant in RCS and WT rats. (**A**) Boxes with a *white* background show average multiunit responses at six individual sites in the SC of an RCS control rat to retinal stimulation with a 200-ms full-field flash. A range of responses is illustrated from very responsive (*top left*) to unresponsive (*bottom right*). Boxes with a *black* background show averaged multiunit responses that were rectified and smoothed. Responses were assigned colors based on their total response area. *Red*: sites with the largest response in that animal; *black*: sites unresponsive to the stimulus. Responses were normalized to the largest response within an animal and color-coded accordingly and a color-coded map (55 sites maximum) of the SC was constructed (**C**) for both IR and visible stimuli for each animal. (**B**) To determine whether each site had a significant stimulus-evoked response, peak amplitude at each site was compared to a criterion level defined as the mean spontaneous activity +6 SEs (High) at that site. Responses that met this criterion were characterized by measuring their onset latency, duration, and total response area. For these computations a baseline criterion was defined as the mean spontaneous activity +2 SEs (Low). Onset latency was defined as the time after stimulus onset when the response exceeded the low threshold. Response duration was the time from onset latency until the response no longer exceeded the low threshold. Total response area was the area under the curve that was bounded by onset latency, duration, and the Low threshold. (**C**) A color-coded SC map documents the spatial distribution of responses to a visible stimulus. (**D**) IR-evoked SC response maps from three representative RCS rats and (**E**) from three WT rats with active implants, along with the average of all animals tested in these two groups. IR responses were evoked in a small area that corresponded to the surgical placement of the ASR in the retina. Response maps are normalized within an animal and do not reflect differences between WT and RCS rats, which are shown instead in Table 3. (**F**) The homogeneous black SC map illustrates the absence of IR-elicited responses at any SC site in any control rat (WT, RCS inactive implant, RCS sham surgery, RCS untreated).

to IR and visible were from matched sites. This excluded only seven IR responsive sites out of a total of 39 in RCS rats. We used Student's *t*-tests (paired and unpaired) to determine whether the presence of implant activity altered visible responses. We compared visible response characteristics at sites with and without IR-evoked activity in WT and in RCS rats. To compare the distribution of visual activity across the SC, we computed the percentage of sites recorded in each rat that had responses to the visible stimulus. An overall mean for RCS with active implants and for each RCS control group (with inactive implants, with sham-surgery, or untreated) was computed, and group means were compared using a one-way ANOVA with post hoc Tukey tests. For comparisons across the three RCS control groups, we defined two SC regions: one corresponding to a region most likely to contain the inactive implant site or surgical site and a second region least likely to contain these sites. To compare across the three RCS controls and these two areas, we used a two-way ANOVA with post hoc Tukey tests to analyze differences across control conditions.

RESULTS

IR Stimulation Evokes ASR-Mediated Signals in RCS Rats with Active Implants

We assessed the ability of the implant to elicit activity under high mesopic conditions using a full-field IR stimulus. This stimulus selectively activates the implant and not native photoreceptors (see Figs. 1, 2F). Figures 2D and 2E plot SC response maps, using the total response area, evoked by the full-field IR stimulus for three representative animals in each group and the overall average maps of RCS and WT rats with active implants. We observed an IR-evoked response only in rats with active implants. Among them, all WT (5/5) and 64% of RCS (9/14) show sites with IR-evoked activity. In contrast, none of the RCS or WT controls showed evidence of any IR-evoked activity (Fig. 2F). In the five WT rats with active implants, we found 51 IR responsive sites and 39 sites were recorded in nine RCS rats with active implants. To verify that

this activity originated in the retina with the active implant, we located and characterized the IR- and visible-evoked responses in an RCS rat with an active implant, then sectioned the optic nerve of the eye with the implant. In the absence of retinal output, neither IR nor visible responses could be evoked (data not shown). Thus, we conclude IR stimulation induces a current selectively in the implant, which evokes retinal activity. This excitation translates into a neural response in the SC.

In both WT (5/5) and RCS (8/9) rats with active implants, IR-evoked activity was found within the retinal representation of the superior nasal quadrant of the retina corresponding to the retinal site of implant placement. There was, however, one exception. In RCS 7747, the IR-evoked response was localized in the lateral edge of the SC, the representation of the inferior nasal retina. Because an unrecoverable mistake was made in processing these retinas, histologic verification of exact implant locations was not possible and thus the exact cause of this anomalous response cannot be traced. The small and consistent location of the IR-evoked activity (13/14 WT and RCS rats) in the SC corresponding to the implant placement in the retina further supports our conclusion that these responses are implant evoked.

Finally, we compared the response characteristics evoked by IR stimulation between RCS and WT rats with active implants (Table 3). We found that all characteristics that we quantified (onset latency, duration and total response) were similar across the WT and RCS rats with active implants, indicating further, that IR-evoked responses are produced via implant activation.

Altered Visible-Evoked Response Characteristics in RCS Rats with an Active Implant

In addition to activity evoked by IR stimulation, we characterized responses in the SC of WT and RCS rats with active implants using visible stimuli. In these rats, 92% (83/90) of sites that had an IR response also showed a visible response, the remainder of the sites had only an IR response. When separated by genotype, 100% of the sites in the WT and 82% (32/39) of the sites in RCS rats that had IR responses also had visible responses.

To examine the potential effects of the presence of the active implant on visible responses, we compared the characteristics of the IR-elicited responses in both WT and RCS rats with active implants with responses evoked by the visible stimulus at all 83 matched sites. For each response characteristic, the IR-evoked response was significantly different from the visible-evoked response (Table 4; paired *t*-tests; $P < 0.0001$). The visible responses had longer onset latencies and times to peak, longer durations, and greater total areas. Figure 3 illustrates two of these significant differences, plotting onset latency as a function of response duration. Each of these differences between the IR and visible response characteristics parallels the differences between the IR and visible stimuli, where the IR stimulus produces an implant current with a shorter duration, as well as a shorter onset latency and smaller total area. Thus, the IR-evoked response characteristics were more similar to the characteristics of the implant output.

TABLE 3. Infrared-Evoked Response Characteristics

Response Characteristic	Onset Latency	Duration	Total Response
WT: active implants			
Mean	0.020	0.096	0.019
SD	0.016	0.090	0.024
n	51	51	51
RCS: active implants			
Mean	0.024	0.083	0.013
SD	0.044	0.11	0.028
n	39	39	39
P (*t*-test)	0.615	0.513	0.286

TABLE 4. Matched Infrared- vs. Visible-Evoked Response Characteristics

Response Characteristic	Onset Latency	Duration	Total Response
IR-evoked			
Mean	0.02	0.10	0.018
SD	0.017	0.10	0.027
n	83	83	83
Visible-evoked			
Mean	0.075	0.37	0.055
SD	0.071	0.21	0.049
n	83	83	83
P (paired *t*-test)	<0.0001	<0.0001	<0.0001

We also examined the effects of the presence of the implant on visible responses by comparing the visible response characteristics of the 51 sites with IR responses to 106 sites without IR-evoked activity in WT rats with active implants. Similarly, we compared the 32 sites with IR-evoked responses to 187 sites without IR-evoked activity in RCS rats with active implants. In WT rats, there were no significant differences in visible response characteristics between sites with and without IR-evoked input. This indicates, first, that the presence of the implant over the short post-implantation period (~2–3 weeks) does not have deleterious effects on the WT retina. In addition, this result suggests that our visible stimulus does not produce an implant-evoked output that significantly contributes to these responses.

In contrast, when we compared response characteristics at sites with and without IR-evoked input in RCS rats with active implants, we found several significant differences (Fig. 4). At sites that received IR input, response onset latencies were significantly shorter, and total response area was larger than at sites that did not receive IR input ($P = 0.04$; 0.05, respectively; one-tailed *t*-test). Because our WT comparisons did not show an effect of implant input on visible response, we interpret these results in RCS rats with active implants to indicate that the presence of an active implant has a trophic effect that results in improved response characteristics.

Comparisons of Visible Responses across RCS Control Groups

We[87] and others[86,91] have observed previously that there is a general effect of surgery on visual responses in the SC of RCS rats that have undergone surgery similar to the one that we use for implantation. To determine whether the presence of an inactive implant had an effect different from surgery alone we compared responses elicited with a visible stimulus across the three groups of RCS controls. We constructed SC response maps for each animal in the three groups as well as average maps for each group (Fig. 5A). In addition, we also computed and compared the average percentage of sites with visible responses across these controls and in RCS rats with active implants. The histogram in Figure 5C plots the results, which show that only untreated RCS controls have significantly fewer visible response sites ($P < 0.02$), similar to our observations in RCS with fetal retinal transplants.

To investigate further the extent of this effect on the response characteristics of visible-evoked responses in control rats, we compared response characteristics elicited with a

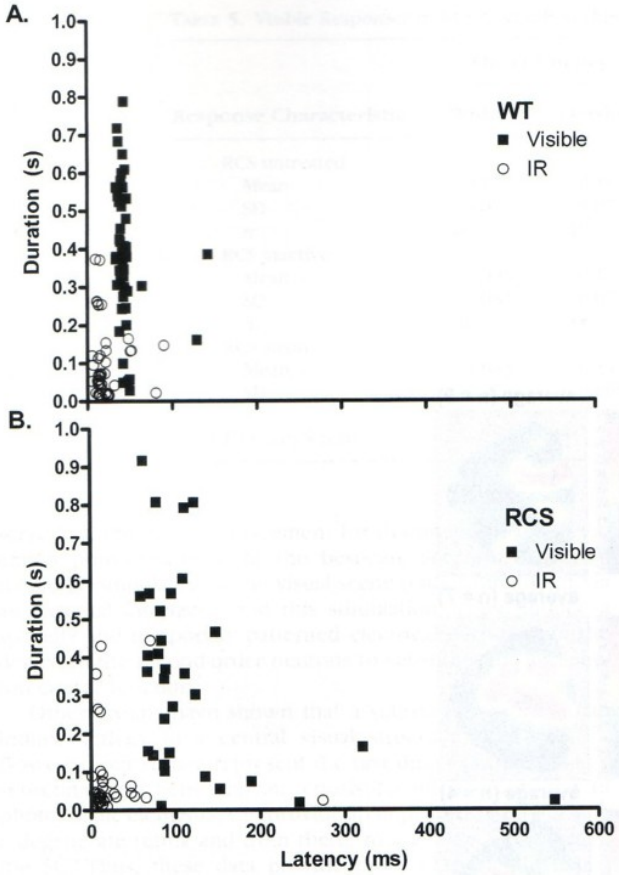

FIGURE 3. IR-evoked responses were significantly different from visible-evoked responses in both WT and RCS rats with active implants. Response duration is plotted as a function of its onset latency for sites that respond to both IR and visible stimuli in (**A**) WT and (**B**) RCS rats with active implants. These scatterplots demonstrate that both of these response characteristics are significantly different when the IR-evoked response is compared to the visible-evoked response (within each plot). In addition, the onset latencies for the visible stimulus are longer when the distribution in the RCS rats is compared to the WT rats (across plots), although the groups do not differ on this response characteristic elicited by the IR stimulus. The faster onset latency elicited with the IR stimulus reflects the rapid response of the ASR device compared with the slower native retinal response to a visible stimulus.

visible stimulus across the control RCS groups. The variability in the locations of sites with IR-evoked responses (in rats with active implants) meant that we could not pinpoint an exact area of inactive implant placement or surgery in these controls. However, we assumed that we could define a region of the SC in the controls, using the location data from WT and RCS with active implants where implant/surgical influence would be most likely and a second region where this influence was least likely. Figure 5A illustrates these regions. We also assumed that there is equal variability between experimental and control groups in the location of sites corresponding to implant placement or surgery.

We compared the same response characteristics between these two regions and also as a function of the control condition: RCS rats with inactive implants, with sham surgery or without treatment (Table 5). We found that the response characteristics in the untreated RCS controls were significantly less robust than in the inactive and sham controls ($P < 0.02$). Further, no significant differences were observed when response characteristics were compared between the two regions, as should be expected, because this is an artificial boundary in the untreated control subjects.

We compared response characteristics between inactive and sham conditions and found that only response duration differed ($P = 0.02$). When responses were compared between areas in the inactive and sham control subjects, we found no significant differences between any of the response characteristics. Thus, although there is a significant effect of surgical intervention on the overall responsiveness of sites in the SC, there is no specific effect on the visible responses within the region corresponding to the site of surgery or the site of the inactive implant. This is in contrast to our results in the RCS rats with active implants, where response characteristics were significantly more robust at sites that received input from the implant.

DISCUSSION

The ultimate goal of subretinal implants is to restore some level of visual perception in patients with degenerative retinal diseases such as RP or AMD. As such, the implant is designed to

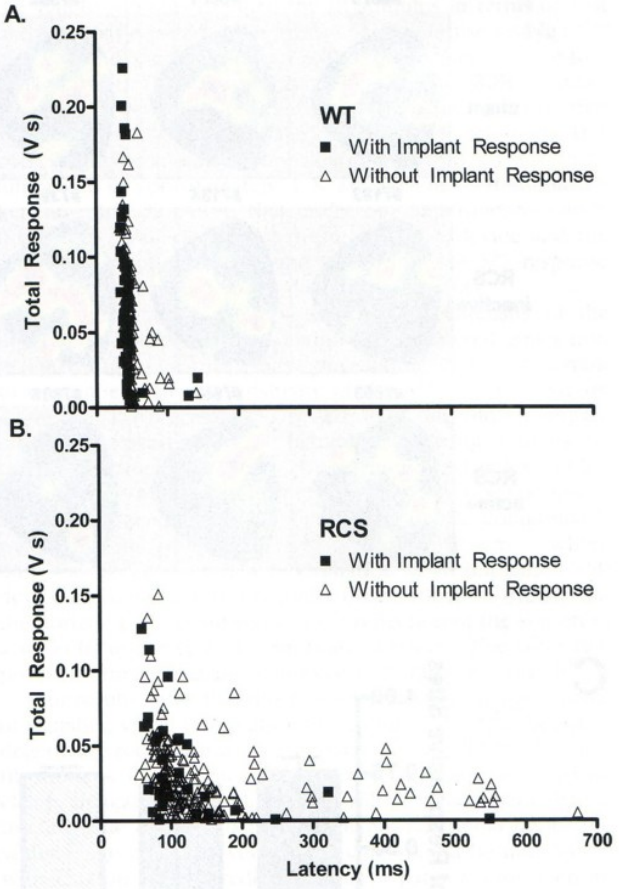

FIGURE 4. Visible responses at sites with implant input differed from responses at sites without implant input in RCS rats and suggest a trophic effect of the active implant. Total response elicited by a visible stimulus is plotted as a function of its onset latency for sites that showed IR-elicited input from the implant and sites that showed no IR-elicited input. (**A**) Response characteristics did not differ in WT rats with active implants when responses at these two types of sites were compared. (**B**) Onset latencies for the visible stimulus are significantly longer and the total response area is significantly smaller in RCS rats at sites without implant input compared with sites with active implant input.

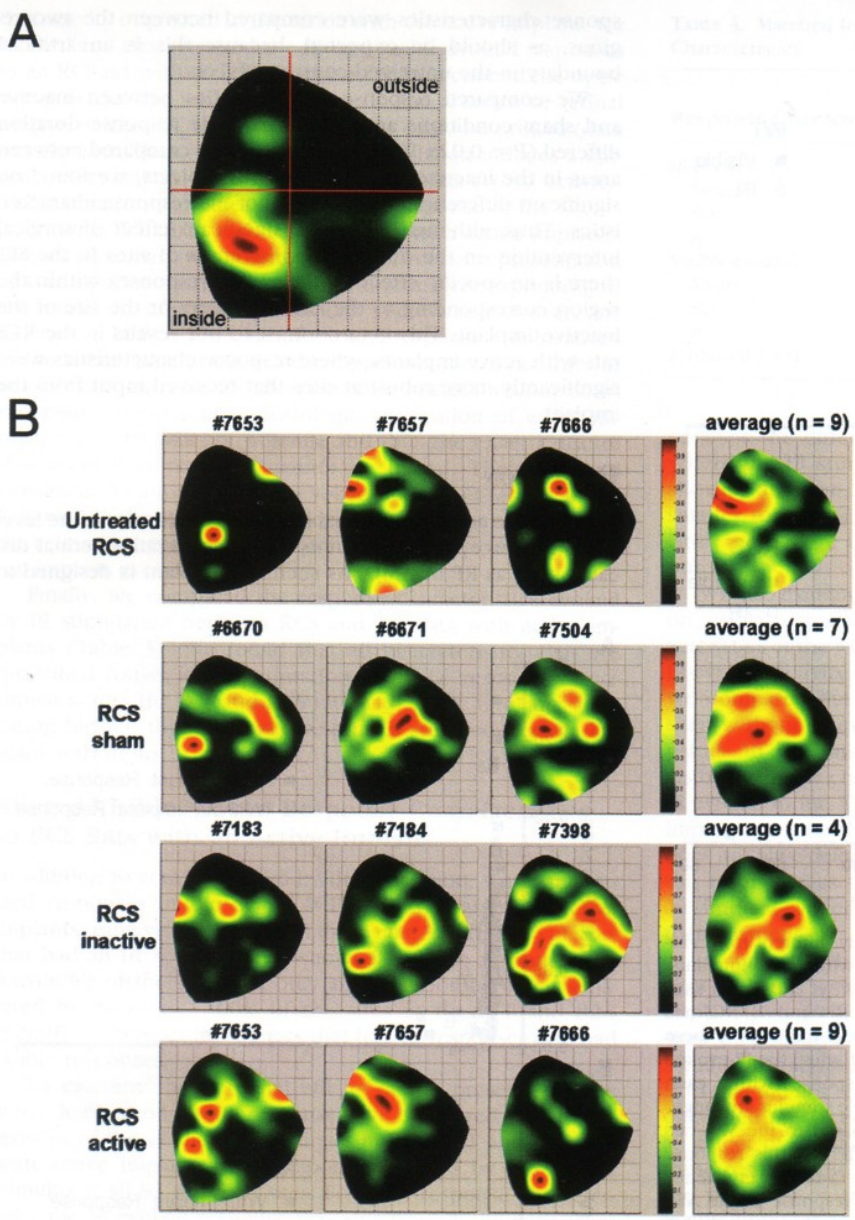

FIGURE 5. A general increase in the number of SC sites with visible responses is seen in all RCS groups with surgery. (**A**) Average SC response map from RCS rats with active implants used to define a region with a high likelihood (inside) and another region with a low likelihood (outside) of containing the site of surgery. (**B**) Three representative SC response maps and an average response map for all rats in the three control groups and in the active implant group. (**C**) The proportion of sites with visible-evoked responses is similar across all groups except in untreated RCS rats, which show a significantly lower proportion of visually responsive sites.

TABLE 5. Visible Responses in RCS Controls within vs. Outside of Potential Implant/Surgical Sites

	Onset Latency		Duration		Total Response	
Response Characteristic	**Within**	**Outside**	**Within**	**Outside**	**Within**	**Outside**
RCS untreated						
Mean	0.17	0.15	0.14	0.16	0.014	0.019
SD	0.07	0.05	0.15	0.20	0.021	0.025
n	60	19	60	19	60	19
RCS inactive						
Mean	0.095	0.1	0.310	0.27	0.042	0.029
SD	0.081	0.07	0.22	0.22	0.036	0.03
n	48	18	48	18	48	18
RCS sham						
Mean	0.083	0.11	0.21	0.26	0.034	0.031
SD	0.074	0.065	0.17	0.15	0.033	0.025
n	94	19	94	19	94	19
P (Tukey's test)	<0.0001		0.025		<0.0001	

serve as a functional replacement for dysfunctional or degenerated photoreceptors. In the best-case scenario, a device would be stimulated by the visual scene (either directly or via an external interface), and this stimulation would induce a spatially and temporally patterned electrical output from the device to the second-order neurons to substitute for lost photoreceptor function.

Other groups have shown that a subretinal electrode can induce activity in a central visual structure.[59,74–77,83,92–94] However, our results represent the first direct evidence that a subretinal prosthetic implant, consisting solely of an array of photovoltaic elements, can provide an implant-evoked signal in a degenerate retina and from there, to a central visual target, the SC. Thus, these data provide proof of principle that a subretinal device can be used to provide some level of visual transduction in a retina with photoreceptor degeneration and subsequent stimulation of central pathways. When IR- and visible-evoked responses were compared at matched sites in WT rats with active implants, the IR-evoked response characteristics were more similar to the implant output characteristics than were the responses evoked by the visible stimulus. This difference is consistent with our other results and argues that the IR light stimulates only the implant.

Although we show empirically that a subretinal photodiode array is capable of inducing central activity, an important consideration is the amount of light that reaches the implant in the subretinal space. To estimate this value for our IR stimulus, we considered both the output of our stimulator and the physiological optics of the rat's eye. Because the sensitivity of the ASR is different from that of the eye, we used radiometric measures in these computations. In addition, we used a simple model of the rat's eye, which considers its geometrical optics and the transmittance of the ocular media. In this model, the irradiance of the retina is related to the irradiance of the cornea by the factor $(T/2) \cdot (r/f)^2$, where r is the pupil radius and f is the focal length of the rat's eye, which we evaluated using a pupil radius of 1.4 mm, a power of 300 D,[95] and a transmittance factor T of 0.75. The IR flash produced by our diffuse source delivers 87 $mW \cdot cm^{-2}$ at the rat cornea, and using our model, we estimate that this flash produces a retinal irradiance of 5.8 $mW \cdot cm^{-2}$. The responsivity of the ASR device is 0.34 $A \cdot W^{-1}$ at 870 nm, so the resultant photocurrent density is $(0.34\ A \cdot W^{-1})(5.8\ mW \cdot cm^{-2}) = 2.0\ mA \cdot cm^{-2}$. It should be noted, however, the proportion of the total photocurrent produced by the device that is delivered as stimulus current to the retina depends on several factors, including both the photocurrent density and the patency of the interface between the device and the retina. Thus, our estimate of 2.0 $mA \cdot cm^{-2}$ of photocurrent should be regarded as an upper bound for the stimulus current produced by our IR stimulus.

Another question is, what brightness would be required for the visible stimulus to equal the IR stimulus in terms of ASR output—that is, what is the irradiance of a diffuse visible (470 nm) flash sufficient to elicit an ASR photocurrent equal to that evoked by our IR stimulus? Taking into account the responsivity of the device at the relevant wavelengths, we estimate that 150 $mW \cdot cm^{-2}$ would be needed. In photometric units, this corresponds to an illuminance of approximately 10^5 lux and a luminance of approximately 3×10^4 $cd \cdot m^{-2}$. It should be kept in mind, however, that under our experimental conditions, this stimulus would activate both the device and the remaining photoreceptors and therefore, the SC response would result from a combination of these inputs.

It is tempting to attempt to relate the intensity of the equivalent visible stimulus to stimuli encountered under normal environmental conditions. When doing so, it is important to remember that the sensitivity of the ASR and the eye are dissimilar and therefore, to be accurate one must compare intensity measurements of naturally occurring sources reported in radiometric units. Documented examples, which bracket our estimates, include (1) The brightest objects viewed in a sunlit scene under cloudless atmospheric conditions,[96] where the total irradiance of the sun is ~50 $mW \cdot cm^{-2}$ (where only wavelengths relevant to excitation of an implanted ASR device are considered); (2) direct observations of the sun on the horizon (e.g., at sunset) and (3) reflection of the sun off of a smooth surface (e.g., a calm body of water). The latter two produce retinal irradiances in excess of 100 $mW \cdot cm^{-2}$.[97]

Our results show that this passive implant design is capable of signaling visual information to central visual structures in a degenerate rodent retina. A comparison of the intensity of our IR stimulus to the intensity of some environmental stimuli clearly indicate that modifications will be needed to enhance this intrinsic output, to make implants functional under the wider range of light levels. These data should be interpreted with caution when predicting what a patient with such an implant would experience. First, the retinal degeneration may have a different underlying etiology and therefore may produce a different implant–retina interface. Further, the stage of degeneration when implants are placed in rodents and humans probably differs and could have a substantial effect on outcome. Behavioral experiments in this rodent model, using IR and visible stimuli at and below the intensity used herein, are needed to determine the answer empirically. In addition, other experiments are necessary to assess whether the device provides spatially and temporally meaningful information.

In addition to the evidence of direct stimulation via the prosthetic, our results argue that there are two trophic effects resulting from the active implant and from the surgical procedure. First, we find that surgery (in either sham or inactive implant) enhances the proportion of visually responsive sites throughout the SC compared with untreated, age-matched RCS rats. This effect of surgery is identical with our observations in RCS rats with fetal retinal transplants.[87] It should be noted that a similar trophic effect was not evident when transgenic S334ter-line 3 rats were examined with similar transplants.[88] This difference may be an important factor when predicting the outcome of implant effectiveness in other models of RP (e.g., rodent, pig, dog, or human).

The second trophic effect is related to the electrical activity produced by the active implant. Visible-evoked response characteristics in RCS rats at sites with input from active implants were significantly more robust than those at sites without this input. This effect was not evident in either RCS rats with inactive implants or with sham surgery; thus, it is specifically related to input from an active implant, a result consistent with observations that have been made on alterations in retinal morphology (Kim MK et al. *IOVS* 2006;47:ARVO E-Abstract 1070).[86] Further, the effect is not evident in WT rats with active implants, consistent with the idea that in WT rats a trophic effect should be difficult to induce and/or demonstrate. These data do not distinguish the mechanism by which this effect occurs. The effect could result from current provided by the implant that supplements the native retinal response. Alternatively, electrical output could induce a trophic effect on the retinal circuitry.

These experiments were designed to characterize functional changes, but not the morphologic correlates underlying these changes. However, other studies have noted an increase in the number of photoreceptor nuclei adjacent to the implant,[86,91] which could enhance the implant–retina interface and result in more robust responses. In addition, the presence of implant activity, itself, could delay or even prevent the process of retinal degeneration (Kim MK et al. *IOVS* 2006;47: ARVO E-Abstract 1070) or reorganization that has been observed in human[98] and mouse models of RP.[99] Because we observe two different trophic influences, it is possible that both processes interact to sustain retinal function.

These data are important because they establish that a subretinally implanted prosthetic device can make a functional interface with a degenerate retina and produce a signal that is transmitted from the retina to a central visual target. This is a critical first step in understanding the conditions required for a functional implant–retina interface and begins to define how a signal from such a device may be used by the retina to produce a meaningful visual percept.

Acknowledgments

The authors thank Machelle Pardue and Neal Peachey for critical comments on the manuscript, Allison Crosby for technical assistance, and Gislin Dagnelie and Mariana Figueiro for productive discussions regarding the characterization of environmental stimuli.

References

1. Chader GJ. Animal models in research on retinal degenerations: past progress and future hope. *Vision Res*. 2002;42:393–399.
2. Mendes HF, van der Spuy J, Chapple JP, Cheetham ME. Mechanisms of cell death in rhodopsin retinitis pigmentosa: implications for therapy. *Trends Mol Med*. 2005;11:177–185.
3. D'Cruz PM, Yasumura D, Weir J, et al. Mutation of the receptor tyrosine kinase gene Mertk in the retinal dystrophic RCS rat. *Hum Mol Genet*. 2000;9:645–651.
4. Lee D, Geller S, Walsh N, et al. Photoreceptor degeneration in Pro23His and S334ter transgenic rats. *Adv Exp Med Biol*. 2003; 533:297–302.
5. LaVail MM, Unoki K, Yasumura D, et al. Multiple growth factors, cytokines, and neurotrophins rescue photoreceptors from the damaging effects of constant light. *Proc Natl Acad Sci USA*. 1992; 89:11249–11253.
6. Delyfer MN Leveillard T, Mohand-Said S, et al. Inherited retinal degenerations: therapeutic prospects. *Biol Cell*. 2004;96:261–269.
7. Doonan F, Cotter TG. Apoptosis: a potential therapeutic target for retinal degenerations. *Curr Neurovasc Res*. 2004;1:41–53.
8. Auricchio A, Rolling F. Adeno-associated viral vectors for retinal gene transfer and treatment of retinal diseases. *Curr Gene Ther*. 2005;5:339–348.
9. Rolling F. Recombinant AAV-mediated gene transfer to the retina: gene therapy perspectives. *Gene Ther*. 2004;11(suppl 1):S26–S32.
10. Nour M, Naash MI. Mouse models of human retinal disease caused by expression of mutant rhodopsin: a valuable tool for the assessment of novel gene therapies. *Adv Exp Med Biol*. 2003;533:173–179.
11. Dinculescu A, Glushakova L, Min SH, Hauswirth WW. Adeno-associated virus-vectored gene therapy for retinal disease. *Hum Gene Ther*. 2005;16:649–663.
12. Aramant RB, Seiler MJ. Progress in retinal sheet transplantation. *Prog Retin Eye Res*. 2004;23:475–494.
13. Seiler MJ, Aramant RB. Transplantation of neuroblastic progenitor cells as a sheet preserves and restores retinal function. *Semin Ophthalmol*. 2005;20:31–42.
14. Das AM, Zhao X, Ahmad I. Stem cell therapy for retinal degeneration: retinal neurons from heterologous sources. *Semin Ophthalmol*. 2005;20:3–10.
15. Klassen H, Sakaguchi DS, Young MJ. Stem cells and retinal repair. *Prog Retin Eye Res*. 2004;23:149–181.
16. Yu DY, Cringle SJ. Retinal degeneration and local oxygen metabolism. *Exp Eye Res*. 2005;80:745–751.
17. Acland GM, Aguirre GD, Ray J, et al. Gene therapy restores vision in a canine model of childhood blindness. *Nat Genet*. 2001;28:92–95.
18. Vollrath D, Feng W, Duncan JL, et al. Correction of the retinal dystrophy phenotype of the RCS rat by viral gene transfer of Mertk. *Proc Natl Acad Sci USA*. 2001;98:12584–12589.
19. Ali RR, Sarra GM, Stephens C, et al. Restoration of photoreceptor ultrastructure and function in retinal degeneration slow mice by gene therapy. *Nat Genet*. 2000;25:306–310.
20. Takahashi M, Miyoshi H, Verma IM, Gage FH. Rescue from photoreceptor degeneration in the rd mouse by human immunodeficiency virus vector-mediated gene transfer. *J Virol*. 1999;73:7812–7816.
21. Tschernutter M, Schlichtenbrede FC, Howe S, et al. Long-term preservation of retinal function in the RCS rat model of retinitis pigmentosa following lentivirus-mediated gene therapy. *Gene Ther*. 2005;12:694–701.
22. Pawlyk BS, Smith AJ, Buch PK, et al. Gene replacement therapy rescues photoreceptor degeneration in a murine model of Leber congenital amaurosis lacking RPGRIP. *Invest Ophthalmol Vis Sci*. 2005;46:3039–3045.
23. Jacobson SG, Aleman TS, Cideciyan AV, et al. Identifying photoreceptors in blind eyes caused by RPE65 mutations: prerequisite for human gene therapy success. *Proc Natl Acad Sci USA*. 2005;102: 6177–6182.
24. Pang J, Cheng M, Stevenson D, et al. Adenoviral-mediated gene transfer to retinal explants during development and degeneration. *Exp Eye Res*. 2004;79:189–201.
25. Chan F, Bradley A, Wensel TG, Wilson JH. Knock-in human rhodopsin-GFP fusions as mouse models for human disease and targets for gene therapy. *Proc Natl Acad Sci USA*. 2004;101:9109–9114.
26. Weber M, Rabinowitz J, Provost N, et al. Recombinant adeno-associated virus serotype 4 mediates unique and exclusive long-term transduction of retinal pigmented epithelium in rat, dog, and nonhuman primate after subretinal delivery. *Mol Ther*. 2003;7: 774–81.
27. Zeng Y, Takada S, Kjellstrom K, et al. RS-1 gene delivery to an adult Rs1h knockout mouse model restores ERG b-wave with reversal of

the electronegative waveform of X-linked retinoschisis. *Invest Ophthalmol Vis Sci*. 2004;45:3279–3285.

28. Lund RD, Adamson P, Sauve Y, et al. Subretinal transplantation of genetically modified human cell lines attenuates loss of visual function in dystrophic rats. *Proc Natl Acad Sci USA*. 2001;98:9942–9947.
29. Mohand-Said S, Hicks D, Dreyfus H, Sahel JA. Selective transplantation of rods delays cone loss in a retinitis pigmentosa model. *Arch Ophthalmol*. 2000;118:807–811.
30. Sauve Y, Girman SV, Wang S, Keegan DJ, Lund RD. Preservation of visual responsiveness in the superior colliculus of RCS rats after retinal pigment epithelium cell transplantation. *Neuroscience*. 2002;114:389–401.
31. Sakaguchi DS, Van Hoffelen SJ, Theusch E, et al. Transplantation of neural progenitor cells into the developing retina of the Brazilian opossum: an in vivo system for studying stem/progenitor cell plasticity. *Dev Neurosci*. 2004;26:336–345.
32. Bok D, Yasumura D, Matthes MT, et al. Effects of adeno-associated virus-vectored ciliary neurotrophic factor on retinal structure and function in mice with a P216L rds/peripherin mutation. *Exp Eye Res*. 2002;74:719–735.
33. Frasson M, Picaud S, Léveillard T, et al. Glial cell line-derived neurotrophic factor induces histologic and functional protection of rod photoreceptors in the rd/rd mouse. *Invest Ophthalmol Vis Sci*. 1999;40:2724–2734.
34. Steinberg RH. Survival factors in retinal degenerations. *Curr Opin Neurobiol*. 1994;4:515–524.
35. Tao W, Raz D, Chan CC, et al. Encapsulated cell-based delivery of CNTF reduces photoreceptor degeneration in animal models of retinitis pigmentosa. *Invest Ophthalmol Vis Sci*. 2002;43:3292–3298.
36. Amendola T, Fiore M, Aloe L. Postnatal changes in nerve growth factor and brain derived neurotrophic factor levels in the retina, visual cortex, and geniculate nucleus in rats with retinitis pigmentosa. *Neurosci Lett*. 2003;345:37–40.
37. Yu DY, Cringle SJ, Valter K, et al. Photoreceptor death, trophic factor expression, retinal oxygen status, and photoreceptor function in the P23H rat. *Invest Ophthalmol Vis Sci*. 2004;45:2013–2019.
38. Lenzi L, Coassin M, Lambiase A, et al. Effect of exogenous administration of nerve growth factor in the retina of rats with inherited retinitis pigmentosa. *Vision Res*. 2005;45:1491–1500.
39. Gauthier R, Joly S, Pernet V, Lachapelle P, Di Polo A. Brain-derived neurotrophic factor gene delivery to Müller glia preserves structure and function of light-damaged photoreceptors. *Invest Ophthalmol Vis Sci*. 2005;46:3383–3392.
40. Davidson FF, Steller H. Blocking apoptosis prevents blindness in Drosophila retinal degeneration mutants. *Nature*. 1998;391:587–591.
41. Farrar GJ, Kenna PF, Humphries P. On the genetics of retinitis pigmentosa and on mutation-independent approaches to therapeutic intervention. *EMBO J*. 2002;21:857–864.
42. Yi X, Schubert M, Peachey NS, et al. Insulin receptor substrate 2 is essential for maturation and survival of photoreceptor cells. *J Neurosci*. 2005;25:1240–1248.
43. Lewin AS, Drenser KA, Hauswirth WW, et al. Ribozyme rescue of photoreceptor cells in a transgenic rat model of autosomal dominant retinitis pigmentosa. *Nat Med*. 1998;4:967–971.
44. LaVail MM, Yasumura D, Matthes MT, et al. Ribozyme rescue of photoreceptor cells in P23H transgenic rats: long-term survival and late-stage therapy. *Proc Natl Acad Sci USA*. 2000;97:11488–11493.
45. Liu J, Timmers AM, Lewin AS, Hauswirth WW. Ribozyme knockdown of the gamma-subunit of rod cGMP phosphodiesterase alters the ERG and retinal morphology in wild-type mice. *Invest Ophthalmol Vis Sci*. 2005;46:3836–3844.
46. Lau D, McGee LH, Zhou S, et al. Retinal degeneration is slowed in transgenic rats by AAV-mediated delivery of FGF-2. *Invest Ophthalmol Vis Sci*. 2000;41:3622–3633.
47. Liang FQ, Aleman TS, Dejneka NS, et al. Long-term protection of retinal structure but not function using RAAV.CNTF in animal models of retinitis pigmentosa. *Mol Ther*. 2001;4:461–472.
48. Spencer B, Agarwala S, Gentry L, Brandt CR. HSV-1 vector-delivered FGF2 to the retina is neuroprotective but does not preserve functional responses. *Mol Ther*. 2001;3:746–756.
49. Boe GJ, Widner H. Clinical neurotransplantation: core assessment protocol rather than sham surgery as control. *Brain Res Bull*. 2002;58:547–553.
50. Holm S. Going to the roots of the stem cell controversy. *Bioethics*. 2002;16:493–507.
51. Brindley GS. The deformation phosphene and the funnelling of light into rods and cones. *J Physiol*. 1967;188:24P–25P.
52. Carpenter RH. Electrical stimulation of the human eye in different adaptational states. *J Physiol*. 1972;221:137–148.
53. Potts AM, Inoue J, Buffum D. The electrically evoked response of the visual system (EER). *Invest Ophthalmol*. 1968;7:269–278.
54. Humayun MS, de Juan E Jr, Dagnelie G, et al. Visual perception elicited by electrical stimulation of retina in blind humans. *Arch Ophthalmol*. 1996;114:40–46.
55. Humayun MS, de Juan E Jr, Weiland JD, et al. Pattern electrical stimulation of the human retina. *Vision Res*. 1999;39:2569–2576.
56. Humayun MS, Weiland JD, Fujii GY, et al. Visual perception in a blind subject with a chronic microelectronic retinal prosthesis. *Vision Res*. 2003;43:2573–2581.
57. Mahadevappa M, Weiland JD, Yanai D, et al. Perceptual thresholds and electrode impedance in three retinal prosthesis subjects. *IEEE Trans Neural Syst Rehabil Eng*. 2005;13:201–206.
58. Rizzo JF 3rd, Wyatt J, Loewenstein J, Kelly S, Shire D. Methods and perceptual thresholds for short-term electrical stimulation of human retina with microelectrode arrays. *Invest Ophthalmol Vis Sci*. 2003;44:5355–5361.
59. Gekeler F, Kobuch K, Schwahn H N, Stett A, Shinoda K, Zrenner E. Subretinal electrical stimulation of the rabbit retina with acutely implanted electrode arrays. *Graefes Arch Clin Exp Ophthalmol*. 2004;242:587–596.
60. Walter P, Heimann K. Evoked cortical potentials after electrical stimulation of the inner retina in rabbits. *Graefes Arch Clin Exp Ophthalmol*. 2000;238:315–318.
61. Chow AY, Chow VY. Subretinal electrical stimulation of the rabbit retina. *Neurosci Lett*. 1997;225:13–16.
62. Schwahn HN, Gekeler F, Kohler K, et al. Studies on the feasibility of a subretinal visual prosthesis: data from Yucatan micropig and rabbit. *Graefes Arch Clin Exp Ophthalmol*. 2001;239:961–967.
63. Humayun M, Sato Y, Propst R, de Juan E Jr. Can potentials from the visual cortex be elicited electrically despite severe retinal degeneration and a markedly reduced electroretinogram? *Ger J Ophthalmol*. 1995;4:57–64.
64. Fried SI, Hsueh HA, Werblin FS. A method for generating precise temporal patterns of retinal spiking using prosthetic stimulation. *J Neurophysiol*. 2006;95:970–978.
65. Sekirnjak C, Hottowy P, Sher A, Dabrowski W, Litke AM, Chichilnisky EJ. Electrical stimulation of mammalian retinal ganglion cells with multielectrode arrays. *J Neurophysiol*. 2006;95:3311–3327.
66. Margalit E, Thoreson WB. Inner retinal mechanisms engaged by retinal electrical stimulation. *Invest Ophthalmol Vis Sci*. 2006;47:2606–2612.
67. Rizzo JF 3rd, Goldbaum S, Shahin M, Denison TJ, Wyatt J. In vivo electrical stimulation of rabbit retina with a microfabricated array: strategies to maximize responses for prospective assessment of stimulus efficacy and biocompatibility. *Restor Neurol Neurosci*. 2004;22:429–443.
68. Weiland JD, Liu W, Humayun MS. Retinal prosthesis. *Annu Rev Biomed Eng*. 2005;7:361–401.
69. Hossain P, Seetho IW, Browning AC, Amoaku WM. Artificial means for restoring vision. *BMJ*. 2005;330:30–33.
70. Jensen RJ, Ziv OR, Rizzo JF. Responses of rabbit retinal ganglion cells to electrical stimulation with an epiretinal electrode. *J Neural Eng*. 2005;2:S16–S21.
71. Jensen RJ, Ziv OR, Rizzo JF 3rd. Thresholds for activation of rabbit retinal ganglion cells with relatively large, extracellular microelectrodes. *Invest Ophthalmol Vis Sci*. 2005;46:1486–1496.

72. Guven D, Weiland JD, Maghribi M, et al. Implantation of an inactive epiretinal poly(dimethyl siloxane) electrode array in dogs. *Exp Eye Res*. 2006;82:81–90.
73. Guven D, Weiland J D, Fujii G, et al. Long-term stimulation by active epiretinal implants in normal and RCD1 dogs. *J Neural Eng*. 2005;2:S65–S73.
74. Yamauchi Y, Franco LM, Jackson DJ, et al. Comparison of electrically evoked cortical potential thresholds generated with subretinal or suprachoroidal placement of a microelectrode array in the rabbit. *J Neural Eng*. 2005;2:S48–S56.
75. Chow AY, Pardue MT, Chow VY, Perlman JI, Peachey NS. Implantation of silicon chip microphotodiode arrays into the cat subretinal space. *IEEE Trans Neural Syst Rehabil Eng*. 2001;9:86–95.
76. Peyman G, Chow AY, Liang C, Chow VY, Perlman JI, Peachey NS. Subretinal semiconductor microphotodiode array. *Ophthalmic Surg Lasers*. 1998;29:234–241.
77. Sachs HG, Schanze T, Wilms M, et al. Subretinal implantation and testing of polyimide film electrodes in cats. *Graefes Arch Clin Exp Ophthalmol*. 2005;243:464–468.
78. Eisenfeld AJ, LaVail MM, LaVail JH. Assessment of possible transneuronal changes in the retina of rats with inherited retinal dystrophy: cell size, number, synapses, and axonal transport by retinal ganglion cells. *J Comp Neurol*. 1984;223:22–34.
79. Pardue MT, Stubbs EB Jr, Perlman JI, Narfstrom K, Chow AY, Peachey NS. Immunohistochemical studies of the retina following long-term implantation with subretinal microphotodiode arrays. *Exp Eye Res*. 2001;73:333–343.
80. Peachey NS, Chow AY. Subretinal implantation of semiconductor-based photodiodes: progress and challenges. *J Rehabil Res Dev*. 1999;36:371–376.
81. Pardue MT, Ball SL, Phillips MJ, et al. Status of the feline retina after 5 years of subretinal implantation. *J Rehabil Res Dev*. In press.
82. Zrenner E. The subretinal implant: can microphotodiode arrays replace degenerated retinal photoreceptors to restore vision? *Ophthalmologica*. 2002;216(suppl 1):8–20; discussion 52–53.
83. Eckhorn R, Wilms M, Schanze T, et al. Visual resolution with retinal implants estimated from recordings in cat visual cortex. *Vision Res*. 2006;46:2675–2690.
84. Javaheri M, Hahn DS, Lakhanpal RR, Weiland JD, Humayun MS. Retinal prostheses for the blind. *Ann Acad Med Singapore*. 2006; 35:137–144.
85. Ball SL, Pardue MT, Chow AY, Chow VY, Peachey NS. Subretinal implantation of photodiodes in rodent models of photoreceptor degeneration. In: Hollyfield JG, Anderson RE, LaVail MM, eds. *New Insights into Retinal Degenerative Diseases*. New York: Kluwer/Plenum Press; 2001:175–180.
86. Pardue MT, Phillips MJ, Yin H, et al. Neuroprotective effect of subretinal implants in the RCS rat. *Invest Ophthalmol Vis Sci*. 2005;46:674–682.
87. Woch G, Aramant RB, Seiler MJ, Sagdullaev BT, McCall MA. Retinal transplants restore visually evoked responses in rats with photoreceptor degeneration. *Invest Ophthalmol Vis Sci*. 2001;42:1669–1676.
88. Sagdullaev BT, Aramant RB, Seiler MJ, Woch G, McCall MA. Retinal transplantation-induced recovery of retinotectal visual function in a rodent model of retinitis pigmentosa. *Invest Ophthalmol Vis Sci*. 2003;44:1686–1695.
89. Siminoff R, Schwassmann HO, Kruger L. An electrophysiological study of the visual projection to the superior colliculus of the rat. *J Comp Neurol*. 1966;127:435–444.
90. Mrsic-Flogel TD, Hofer SB, Creutzfeldt C, et al. Altered map of visual space in the superior colliculus of mice lacking early retinal waves. *J Neurosci*. 2005;25:6921–6928.
91. Pardue MT, Phillips MJ, Yin H, et al. Possible sources of neuroprotection following subretinal silicon chip implantation in RCS rats. *J Neural Eng*. 2005;2:S39–S47.
92. Sachs HG, Schanze T, Brunner U, Sailer H, Wiesenack C. Transscleral implantation and neurophysiological testing of subretinal polyimide film electrodes in the domestic pig in visual prosthesis development. *J Neural Eng*. 2005;2:S57–S64.
93. Salzmann J, Linderholm OP, Guyomard JL. Subretinal electrode implantation in the P23H rat for chronic stimulations. *Br J Ophthalmol*. 2006;90:1183–1187.
94. Schanze T, Sachs HG, Wiesenack C, Brunner U, Sailer H. Implantation and testing of subretinal film electrodes in domestic pigs. *Exp Eye Res*. 2006;82:332–340.
95. Hughes A. A schematic eye for the rat. *Vision Res*. 1979;19:569–588.
96. ASTM G173-03e1. *Standard Tables for Reference Solar Spectral Irradiances: Direct Normal and Hemispherical on 37° Tilted Surface*. West Conshohocken, PA: ASTM International; 2003.
97. Sliney D, Wolbarsht H. *Safety with Lasers and Other Optical Sources: a Comprehensive Handbook*. New York: Plenum Press; 1980.
98. Jones BW, Marc RE. Retinal remodeling during retinal degeneration. *Exp Eye Res*. 2005;81:123–137.
99. Strettoi E, Pignatelli V, Rossi C, Porciatti V, Falsini B. Remodeling of second-order neurons in the retina of rd/rd mutant mice. *Vision Res*. 2003;43:867–877.